Synthesis and Characterization of Erbium Trioxide Nanoparticles as Photo-Catalytic for Degradation of Methyl Orange Dye

Rifat Mohammed Dakhil[1], Tayser Sumer Gaaz[2], Ahmed Al-Amiery[3,*] Mohd S. Takriff[3] and Abdul Amir H. Kadhum[3,]

1 Technical College Basra, Southern Technical University, Iraq

2 Department of Machinery Equipment Engineering Techniques, Technical College Al-Musaib, Al-Furat Al Awsat Technical University, Al-Musaib, Babil 51009, Iraq

3 Department of Chemical & Process Engineering, Faculty of Engineering & Built Environment, Universiti Kebangsaan Malaysia, Bangi, Selangor 43600, Malaysia

***** Correspondence: dr.ahmed1975@gmail.com

ABSTRACT

The present work focuses on the photo-catalytic degradation of methyl orange (MO) on Erbium trioxide nanoparticles "Er_2O_3 NPs". In this study, Er_2O_3 nanoparticles were synthesized and fully characterized via various techniques including; XRD diffraction, UV-Vis spectroscopy and SEM techniques. The results revealed that, the photo-catalytic activity of the prepared Er_2O_3 NPs towards methyl orange (MB) photo-degradation was manifested. The optimum efficiency obtained was 16%.

Keywords: methyl orange; Er_2O_3; Photo-catalytic; XRD; SEM Nomenclature

1 Introduction

One of the sources of water contamination was the wastewater generated from textile-plants employing various dyestuffs (Khataee and Kasiri, 2010; Barbe et al., 1997). Various chemical and physical in addition to biological changes for dyes could occur that consume dissolved oxygen in the water bodies. Moreover, dyes have high toxicity which endangers aquatic life (Khataee et al., 2009; Ruiz et al., 2004). The various traditional techniques employed for the processing of pollutants textile dyes in water involve different chemical, biological and/or physical techniques. Photo-catalytic degradation was demonstrate as a promising technique for processing of pollutions that occur due to organic and/or inorganic compounds. The approach,

as a means of removal of persistent water contaminants like dyes and pesticides was attracted recently the attention of numerous investigators (Xu et al., 2014; Chen et al., 2014; Liu et al., 2014). Considerable of these researchers were used suspension (aqueous) of semi-conductors irradiated by UV-light to photo-degrade the pollutants (Daneshvar et al., 2007). The accomplishment of a semi-conductor photo-catalyst was strongly connected with the electronic structure of it (Daneshvar et al., 2007; Boppella et al., 2013; Xiao et al., 2012; Alenezi et al., 2013). It was established that the photo-catalytic degradation of organic ions or organic molecules in solution are launched by photo-generated holes in valence band with electrons in the conduction band of the semi-conductor photo-catalyst. The generated holes have high oxidative potential that permits a direct oxidation of organic ions or organic molecules to reactive intermediates. Moreover, radicals are reactive species that may help in organic substrate degradation. Methyl orange as in Fig. 1, is a scale of acidity utilized in titration due to its clear and distinct color difference at various pH values. Methyl orange demonstrates pink colour in acidic solution and yellow colour in basic solution. Due to it variations colour at the pH of a mid-strength acid, it is ordinarily utilized in titration for acid solutions. Unlike a global indicator, methyl orange does not have a full spectrum of colour variation, but it has a sharp end (Khodja et al., 2001; Sandberg et al., 1972).

Fig. 1

Generally, MO utilized monoazo dye in laboratory tests, textiles and different commercial products and has to be eliminate from water because of its toxicity (Mittal et al., 2007; Chen et al., 2010). Mittal et al. (Mittal et al., 2007) searched the eliminate and recovery of MO from wastewaters employing waste materials. Chen and his co-workers (Chen et al., 2010) examined the equilibrium and kinetic aspects of MO adsorption on activated carbon derived from Phragmites austral is. Jiang and other researchers (Jiang et al., 2012) investigated the removal of MO from solutions through Maghemite-Chitosan NPs. Therefore, there is a need to develop a novel treatment method that is more effective in eliminating dyes from the wastewater. The objective and novelty of the present work is to study the factors effecting on photo-catalytic oxidation process of methyl orange dye using the synthesized erbium trioxide Nanoparticles such as concentration, illumination time and amount of catalyst loaded used in photo-catalytic process. In this investigation, we searched the photo-catalytic degradation of MO on Er_2O_3 NPs.

2 Experimental

2.1 Materials

All materials used in this work were supplied from Fluka Company, and were used without further purification.

2.2 Synthesis of Er_2O_3 NPs

Erbium oxide nanoparticles (Er_2O_3 NPs) had been synthesized by dissolving of ascorbic acid (1 g) and of sodium fluoride (0.063 g) in distilled water (10 mL). Adjusted the pH solution to four by adding drops of ammonium hydroxide solution. The resulting solution was heated to 70 ºC for 20 min. An alcoholic solution of Erbium nitrate (2.5 g in 4 mL) had been added to the above solution and continuous stirring 2 hr. At room temperature. Centrifuged and washed the precipitate several times with de-ionized water dried in air for 24 hr under vacuum. The precipitate, then calculated at 800 ºC for 3 hr.

2.3 Sample Preparation

Er_2O_3 nanoparticles were prepared as the catalyst of 0.1 g diluted in 100 mL methanol). Erbium oxide Er_2O_3 and methyl orange (MO) were weighed by using sensitive balance. MO as a dye often used for catalytic tests (0.05 g diluted with 500 mL methanol).

2.4 Photo-Catalytic Setup

The photo-catalytic set-up consists of UV- source as a lamp (6 watt) of cylindrical shape 22 cm body length and 16 cm arc length of cylindrical shape, which was used as a photo source. This was used as a photo source. This lamp was positioned in a container of the sample (mixture of Er_2O_3 NPs and MO) and then placed on magnetic stirrer (to mix and disperse solutions result of high speeds and long time to prepare it solutions) (Chen et al., 2014).

2.5 Methods

2.5.1 Irradiation Time Effect

The Mixture of Er_2O_3 NPs and MO was placed on magnetic stirrer and the temperature was fixed at 25 ºC. The UV-lamp was switched on inside the sample container. Different irradiation time (1, 2, 3, 4 and 5 hr) were employed. The photo degradation measured after each hour. The samples were examined by UV-spectrometer to measure the absorbance of all sample.

2.5.2 Dye Concentration Effect

Different concentrations of the MO were used in the range of (0.1, 0.2, 0.5, 1, 1.5, 2) wt.% and 0.1 wt.% from Er_2O_3 NPs. The samples withdrawn from the mixture without photo catalysts and after 15 minute for each concentration of MO. The samples were examined by UV-visible spectrophotometer to measure the optical absorbance.

2.5.3 Scanning Electron Microscopy (SEM)

The morphology of the nanoparticles of Erbium oxide nanoparticles was studied by SEM. It was recorded on the JEOL JSM-6390LV SEM fitted with secondary electron detector.

2.5.4 X-ray diffraction (XRD)

The crystallinity of Er_2O_3 powder was studied by X-ray diffraction (XRD) technique.

3 Results and Discussion

To improve the photo-degradation efficiency of methyl orange dye, erbium trioxide nanoparticles were used as a common strategy. Erbium trioxide nanoparticles were ready to synthesis and cheap. Various types of nano-metal have been used in the previous studies, including anionic dopants, cationic dopants, rare-earth dopants, and codopants (Samadi et al., 2014). Besides, many studies have shown that coupling with other semiconductors, such as CdO (Liu et al., 2014), CeO2 (Uddin et al., 2012)], SnO2,TiO2 (Pant et al., 2012), graphene oxide (GO) (Dai et al., 2014), and reduced grapheme oxide (RGO) (Zhou et al., 2012), is a feasible approach to enhance the photodegradation efficiency.

3.1 Absences of Sunlight

The results had been discussed with/without sunlight as shown in Figs. 2 and 3. Fig. 2 demonstrates the relation between absorbance and time of photo-catalytic without sunlight radiation. The increasing of time of photo-degradation up to 3.0 hr, leads to that the absorbance values will raise, due to the degradation process organic dye. This attitude harmonize with Lazar et al. (Lazar et al., 2012). Fig. 3 elucidate the absorption of Er_2O_3 spectrum in absence of sun light (SL), that could be shown that the minimum absorption occur at wavelength range of (324-489 nm) for various irradiative time.

Fig. 2

Fig. 3 shows the absorption spectrum of Er_2O_3 nanoparticles without SL. One can be shown that the minimum absorption take place at the range of wavelength (450-600 nm) for different irradiative time. A transmission spectrum has maximum intensities at wavelengths where the absorption is weakest because more light is transmitted through the sample. An

absorption spectrum has maximum intensities at wavelengths where the absorption is strongest. When sample molecules are exposed to light having an energy that matches a possible electronic transition within the molecule, some of the light energy will be absorbed as the electron is promoted to a higher energy orbital. An optical spectrometer records the wavelengths at which absorption occurs, together with the degree of absorption at each wavelength. Absorbance usually ranges from 0 to 3.5, and is precisely defined in context with spectrometer operation.

Fig. 3

3.2 In presence of SL

Fig. 4 shows the photo-catalytic degradation of diazocompounds irradiated under sunlight in the presence of Er_2O_3 nanoparticles. The presence of Er_2O_3 nanoparticles was investigated as a very important factor for improvement the degradation process. Higher efficiency of degradation was found within 4.0 hr, of irradiation time and considering the optimum loading of catalyst. After 4.0 hr, of irradiation time with Er_2O_3 nanoparticles, can be shown other peak at irradiation time of 5.0 hr, when we carried out a comparison between the absorbance values at 5 hr. with Fig. 2 and without sunlight can be conclude the improvement in phenolic compound degradation when taken into account the role of sunlight.

Fig. 4

The rate of reaction increases and maximum rates were getting after four hour as shown in Fig. 5. It may be explained on the basis that the operation time of UV source was increased, the number of photons per unit area incident on the sample also increased, resulting in high rate of degradation in the mixture of Erbium oxide and MO Leads to increase the absorption value.

Fig. 5

3.3 Impact of Methylene Blue Concentration

3.3.1 Concentration of MO Effects without Irradiation

The increasing in the dye concentration leads to increases of absorbance. The maximum change of absorbance increasing was noticed when the concentration changed from 0.5 wt.% to 1wt.%

as shown in Fig. 6. The degradation efficiency of MO was analyzed using UV-Vis spectrometer. Peaks were observed to be present between 450 and 600 nm, which was indicative of the degradation of MO. According to Beer-Lambert Law, MO concentration is directly proportional to its absorbance (Ramli et al., 2014).

3.3.2 Concentration of MO Effects with Irradiation

When MO concentration increased leads to the value of absorbance was increased after 15 min from irradiation. Maximum increasing in absorbance notice when changed the concentration at the period (0.5-1.0) wt.% as shown in Fig. 6. This might be elucidated base on the increasing of dye concentrations that leads to the reaction average increases as additional, molecules. When increased the dye (3.0-5.0) wt.% the value of absorbance remains constant at 4.51 wt.% cause reaction retardation because of the increasing in number of collisions between dye molecules whereas, collisions between dye and salt decrease. As a conclusion, proportion of reaction was decrease (Karunakaran et al., 2004; Pandey et al., 2015). The main rate of degradation exists in the region near irradiated side where the intensity of irradiation was much higher than in the other sides. Thus, dye with higher concentration, the degradation technique decreases at sufficiently long distances from the light source or the reaction zone because of retardation in the penetration of light.

Fig. 6

3.4 SEM Results

The SEM micrographs of synthesized samples are shown in Figs. 7, 8, 9 and 10, this Figs. show the distribution and the morphology of Er_2O_3 nanoparticles. The average size of the nanoparticles was found to be (~16 nm) and appeared to be uniform.

Fig. 7

Fig. 8

Fig. 9

Fig. 10

3.5 XRD Results

XRD was used to clarify the Er_2O_3 nanoparticles phase formation. All the reflections were well indexed to cubic phase of Er_2O_3 nanoparticles and can be seen from Fig. 11, XRD parameter of Er_2O_3 nanoparticles show in Table 1 with a space group of I 21 3 (199) and cell parameters of a=10.5400 Å. The excellent crystallinity and absence of impurities can be inferred because of sharpness and exact number of peaks in the XRD pattern. Additionally, it indicates that the product is a single phase. XRD was used to clarify the Er_2O_3 nanoparticles phase formation. All the reflections were well indexed to cubic phase of Er_2O_3 nanoparticles, the average crystallite size of Er_2O_3 nanoparticles is found to be 16 nm.

Fig. 11

Table 1

4 Conclusion

Nanoparticles of Er_2O_3 under SL improvement the effectiveness degradation diazomium compounds for methyl orange or in other words removal of mixture polluted by methyl orange. The photo catalytic activity under UV and light illumination, components for the enhanced photo synergist reactivity of the Er_2O_3. The Er_2O_3 nanoparticles have stage and it is ready to ingest a high measure of photo catalytic in the obvious light area, driving adequately photochemical degradation responses. Maximum increasing of absorbance was noticed when the concentration of MO increased from 0.5 wt.% to 1wt.% and this behavior leads to increasing degradation of MO up to 14 % for Er_2O_3 catalyst. XRD measurements show that the structure of Er_2O_3 nanoparticles was Cubic, the average crystallite size of Er_2O_3 nanoparticles is found to be 16 nm.

Acknowledgments

The authors gratefully acknowledge the UKM-YSD Chair on Sustainable Development for the Grant 020–2017 'Malaysia' for supporting this work.

References

Alenezi MR, Alshammari AS, Jayawardena KI, et al. (2013), *The Journal of Physical*
Alenezi, M. R., Alshammari, A. S., Jayawardena, K. I., Beliatis, M. J., Henley, S. J., & Silva, S.: Role of the exposed polar facets in the performance of thermally and UV

223 activated ZnO nanostructured gas sensors, The Journal of Physical Chemistry C,
224 117(34), 17850-17858, https://pubs.acs.org/doi/abs/10.1021/jp4061895, 2013.
225
226 Barbe, C. J., Arendse, F., Comte, P., Jirousek, M., Lenzmann, F., Shklover, V., &
227 Grätzel,
228 M.: Nanocrystalline titanium oxide electrodes for photovoltaic applications, Journal
229 of the American Ceramic Society, 80(12), 3157-3171,
230 https://onlinelibrary.wiley.com/doi/abs/10.1111/j.1151-2916.1997.tb03245.x, 1997.
231
232 Boppella, R., Anjaneyulu, K., Basak, P., & Manorama, S. V.: Facile synthesis of face
233 oriented ZnO crystals: tunable polar facets and shape induced enhanced photocatalytic
234 performance, The Journal of Physical Chemistry C, 117(9), 4597-4605,
235 https://pubs.acs.org/doi/10.1021/jp311443s, 2013.
236
237 Chen, J., Li, S., Ma, S., & Wang, X.: Polar Fuzzy Sets: An Extension of Bipolar Fuzzy
238 Sets, The Scientific World Journal, 2014,
239 https://www.hindawi.com/journals/tswj/2014/416530/abs/, 2014.
240
241 Chen, S., Zhang, J., Zhang, C., Yue, Q., Li, Y., & Li, C.: Equilibrium and kinetic studies
242 of
243 methyl orange and methyl violet adsorption on activated carbon derived from
244 Phragmites australis, Desalination, 252(1-3), 149-156,
245 https://www.sciencedirect.com/science/article/pii/S0011916409012193, 2010.
246
247 Daneshvar, N., Rasoulifard, M., Khataee, A., & Hosseinzadeh, F.: Removal of CI Acid
248 Orange 7 from aqueous solution by UV irradiation in the presence of ZnO
249 nanopowder, Journal of Hazardous Materials, 143(1-2), 95-101,
250 https://www.sciencedirect.com/science/article/pii/S0304389406010405, 2007.
251
252 Dai, K. Lu, L. Liang C., “Graphene oxide modiied ZnO nanorods hybrid with high
253 reusable photocatalytic activity under UV-LED irradiation,” Materials Chemistry and
254 Physics, vol. 143, no. 3, pp. 1410–1416, 2014.
255
256 Jiang, R., Fu, Y. Q., Zhu, H. Y., Yao, J., & Xiao, L.: Removal of methyl orange from
257 aqueous solutions by magnetic maghemite/chitosan nanocomposite films: adsorption
258 kinetics and equilibrium, Journal of Applied Polymer Science, 125(S2), E540-E549,
259 https://onlinelibrary.wiley.com/doi/abs/10.1002/app.37003, 2012.
260
261 Karunakaran, C., Senthilvelan, S., Karuthapandian, S., & Balaraman, K.:
262 Photooxidation of
263 iodide ion on some semiconductor and non-semiconductor surfaces, Catalysis

Communications, 5(6), 283-290, https://www.sciencedirect.com/science/article/pii/S1566736704000470, 2004.

Khataee, A., & Kasiri, M. B.: Photocatalytic degradation of organic dyes in the presence of nanostructured titanium dioxide: influence of the chemical structure of dyes, Journal of Molecular Catalysis A: Chemical, 328(1-2), 8-26, https://www.sciencedirect.com/science/article/pii/S1381116910002384, 2010.

Khataee, A., Pons, M.N., & Zahraa, O.: Photocatalytic degradation of three azo dyes using immobilized TiO2 nanoparticles on glass plates activated by UV light irradiation: Influence of dye molecular structure, Journal of Hazardous Materials, 168(1), 451-457, https://www.sciencedirect.com/science/article/pii/S0304389409002519, 2009.

Khodja, A. A., Sehili, T., Pilichowski, J.-F., & Boule, P.: Photocatalytic degradation of 2-phenylphenol on TiO2 and ZnO in aqueous suspensions, Journal of Photochemistry and Photobiology A: Chemistry, 141(2-3), 231-239, https://www.sciencedirect.com/science/article/abs/pii/S1010603001004233, 2001.

Lazar, M., Varghese, S., & Nair, S.: Photocatalytic water treatment by titanium dioxide: recent updates, Catalysts, 2(4), 572-601, https://www.mdpi.com/2073-4344/2/4/572/htm, 2012.

Liu, B., Zhao, X., Terashima, C., Fujishima, A., & Nakata, K.: Thermodynamic and kinetic analysis of heterogeneous photocatalysis for semiconductor systems, Physical Chemistry Chemical Physics, 16(19), 8751-8760, https://pubs.rsc.org/en/content/articlelanding/2014/cp/c3cp55317e/unauth#!divAbstract, 2014.

Liu,I. Hon, M. and Teoh, L. “hepreparation, characterization and photocatalytic activity of radical-shaped CeO2 /ZnO microstructures,” Ceramics International,vol.40, no.3,pp.4019–4024,2014.

Mittal, A., Malviya, A., Kaur, D., Mittal, J., & Kurup, L.: Studies on the adsorption kinetics and isotherms for the removal and recovery of Methyl Orange from wastewaters using waste materials, Journal of Hazardous Materials, 148(1-2), 229-240, https://www.sciencedirect.com/science/article/pii/S0304389407002518, 2007.

Pandey, A., Kalal, S., Ameta, C., Ameta, R., Kumar, S., & Punjabi, P. B.: Synthesis, characterization and application of naïve and nano-sized titanium dioxide as a photocatalyst for degradation of methylene blue, Journal of Saudi Chemical Society, 19(5), 528-536, https://www.sciencedirect.com/science/article/pii/S1319610315000678, 2015.

Pant, H. Park, C. Pant, P. Tijing, L. Kim, H. and Kim, C. "Synthesis, characterization, and photocatalytic properties of ZnO nano-lower containing TiO2 NPs,"Ceramics International,vol.38,no.4,pp.2943–2950,2012.

Ramli, C., Amali, Z., Asim, N., Isahak, W. N., Emdadi, Z., Ahmad-Ludin, N., Yarmo, M. A., & Sopian, K.: Photocatalytic Degradation of Methylene Blue under UV Light Irradiation on Prepared Carbonaceous, The Scientific World Journal, 2014, https://www.hindawi.com/journals/tswj/2014/415136/abs/, 2014.

Ruiz, A. M., Sakai, G., Cornet, A., Shimanoe, K., Morante, J. R., & Yamazoe, N.: Microstructure control of thermally stable TiO2 obtained by hydrothermal process for gas sensors, Sensors and Actuators B: Chemical, 103(1-2), 312-317, https://www.sciencedirect.com/science/article/pii/S0925400504002503, 2004. 282

Samadi, M. Pourjavadi, A. and Moshfegh, A. "Role of CdO addition on the growth and photocatalytic activity of electrospun ZnO nanoibers: UV vs. visible light," Applied Surface Science , vol. 298, pp. 147–154, 2014.

Sandberg, R. G., Henderson, G. H., White, R. D., & Eyring, E. M.: Kinetics of acid dissociation-ion recombination of aqueous methyl orange, The Journal of Physical Chemistry, 76(26), 4023-4025, https://pubs.acs.org/doi/abs/10.1021/j100670a024?journalCode=jpchax, 1972.

[Uddin, M. Nicolas, Y. Olivier Cl., "Nanostructured SnO2-ZnO heterojunction photocatalysts showing enhanced photocatalytic activity for the degradation of organic dyes," Inorganic Chemistry ,vol.51,no.14,pp.7764–7773,2012.

Xiao, Y., Lu, L., Zhang, A., Zhang, Y., Sun, L., Huo, L., & Li, F.: Highly enhanced acetone sensing performances of porous and single crystalline ZnO nanosheets: high percentage of exposed (100) facets working together with surface modification with Pd nanoparticles, ACS applied materials & interfaces, 4(8), 3797-3804, https://pubs.acs.org/doi/abs/10.1021/am3010303, 2012.

Xu, C., Rangaiah, G., & Zhao, X.: Photocatalytic degradation of methylene blue by titanium
dioxide: experimental and modeling study, Industrial & Engineering Chemistry Research, 53(38), 14641-14649, https://pubs.acs.org/doi/abs/10.1021/ie502367x, 2014.

Zhou, X. Shi, T. and Zhou, H. “Hydrothermal preparation of ZnO-reduced graphene oxide hybrid with high performance in photocatalytic degradation,” Applied Surface Science,vol.258,
no. 17, pp. 6204–6211, 2012.

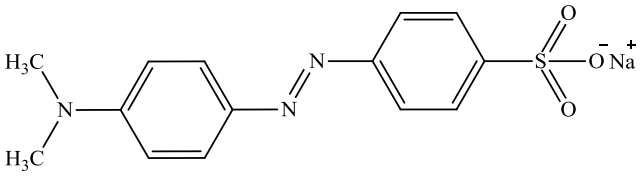

Fig. 1.The chemical structure of methyl orange.

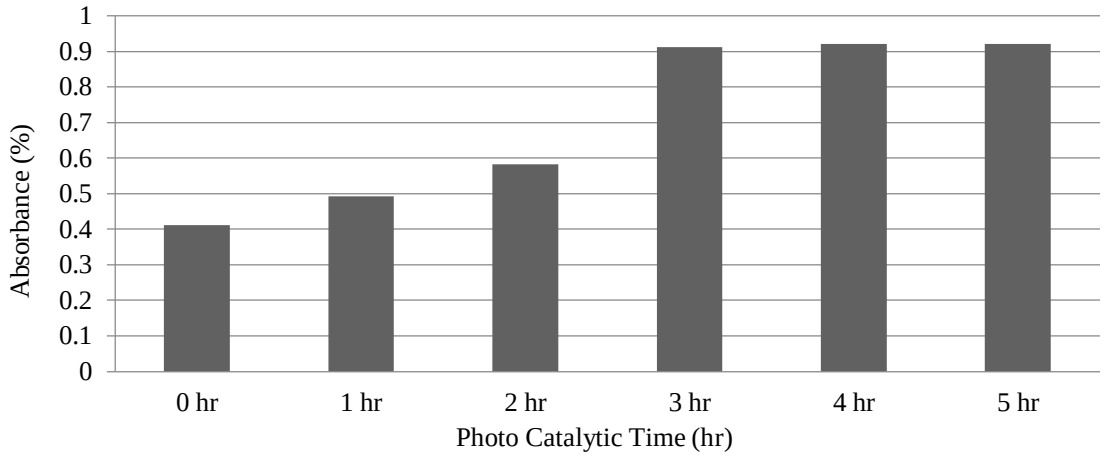

Fig. 2. The photo-catalytic time vs absorbance without SL.

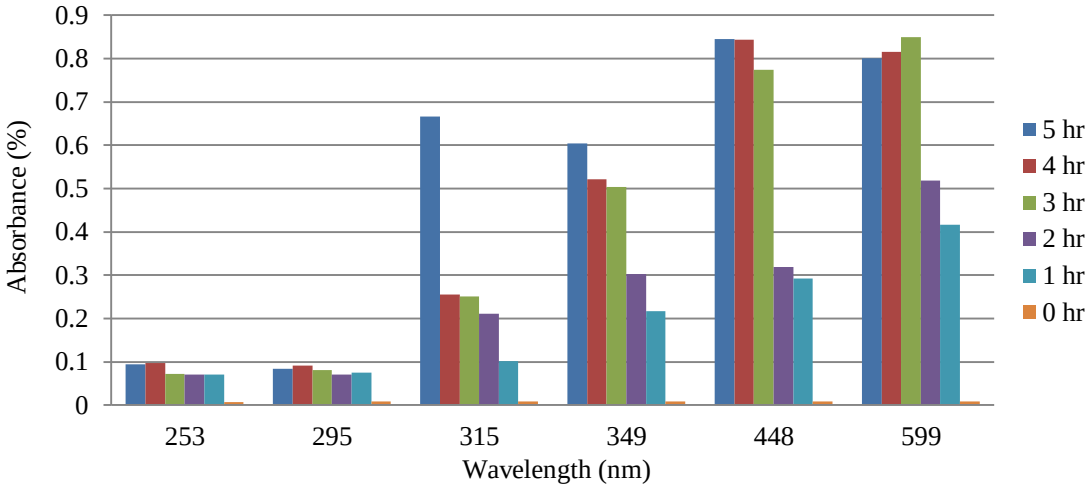

Fig. 3. UV–visible spectra of Er_2O_3 nanoparticles without SL.

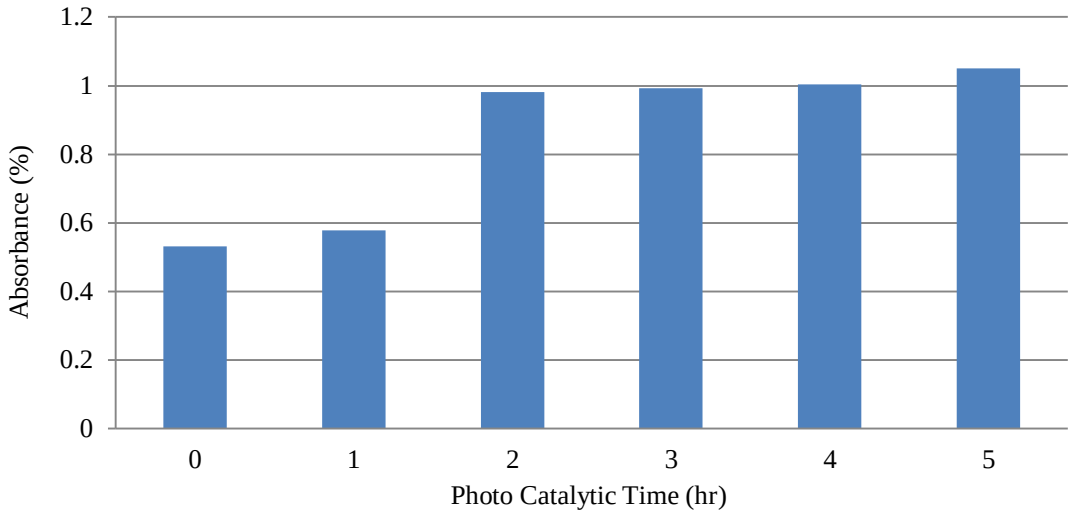

Fig. 4. Photo-catalytic degradation of methylene blue dye over Er_2O_3 samples as a function of irradiation time with SL.

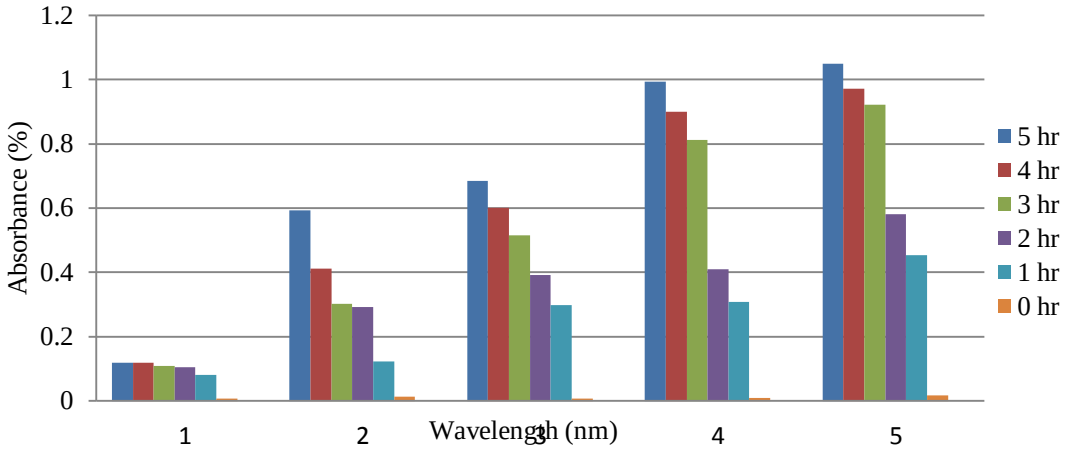

Fig. 5. UV–visible spectra of Er_2O_3 with SL.

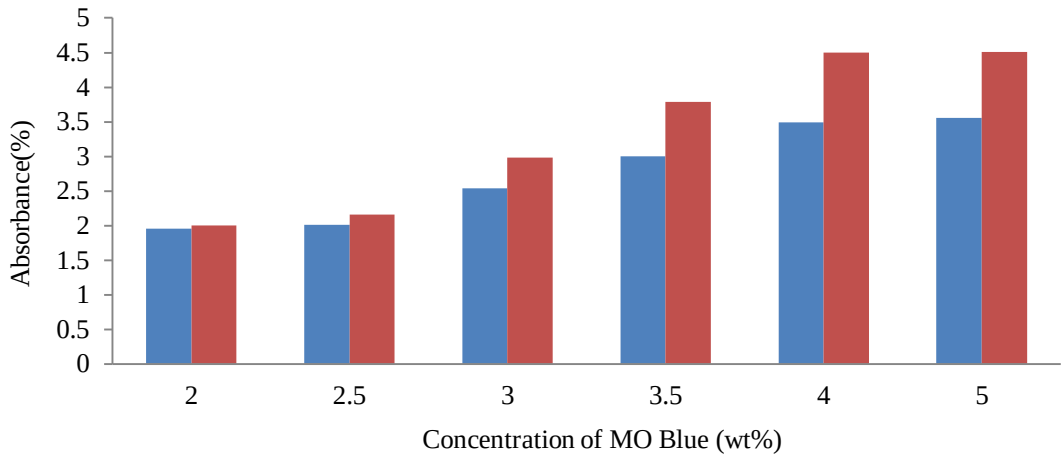

Fig. 6. The concentration of MO dye versus with absorbance, with and without irradiation.

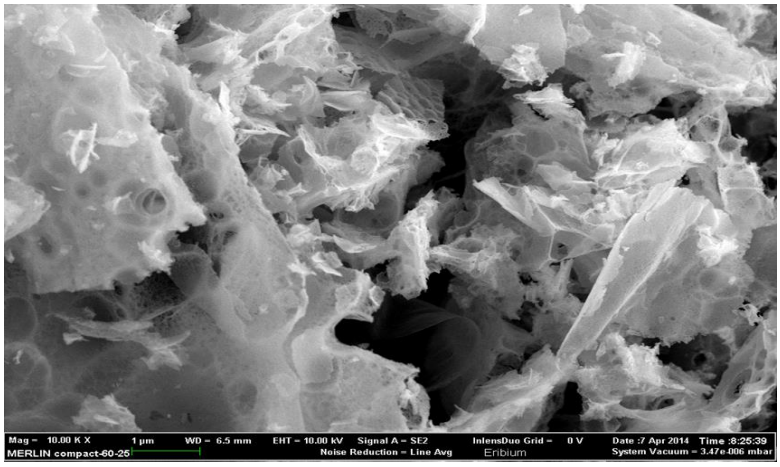

Fig. 7. SEM image shows a distribution of Erbium oxide particles 1000 kx.

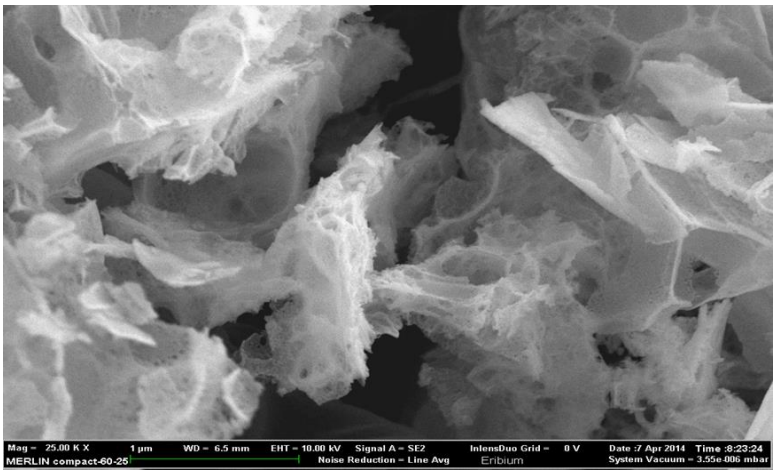

Fig. 8. Shows an even distribution for Erbium oxide particles 2500 kx.

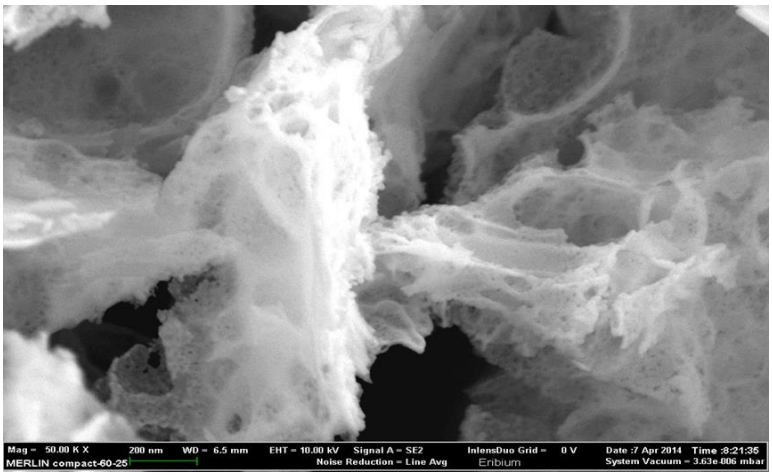

Fig. 9. SEM image of nano-sized Er_2O_3 5000 kx.

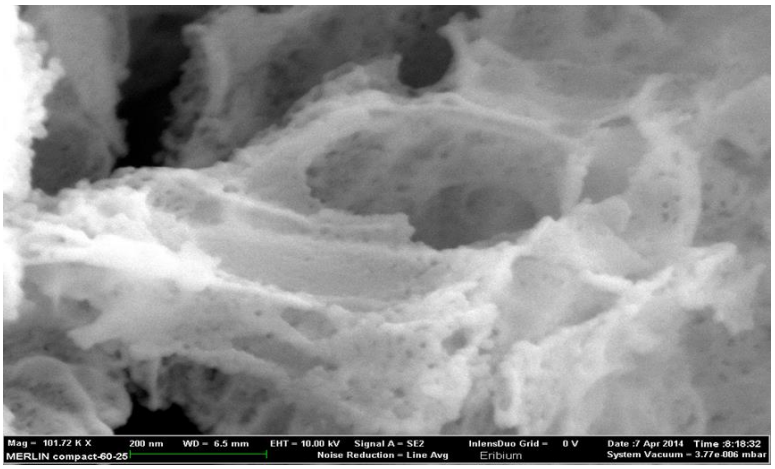

Fig. 10. SEM image of nanosized Er_2O_3 101.72 kx.

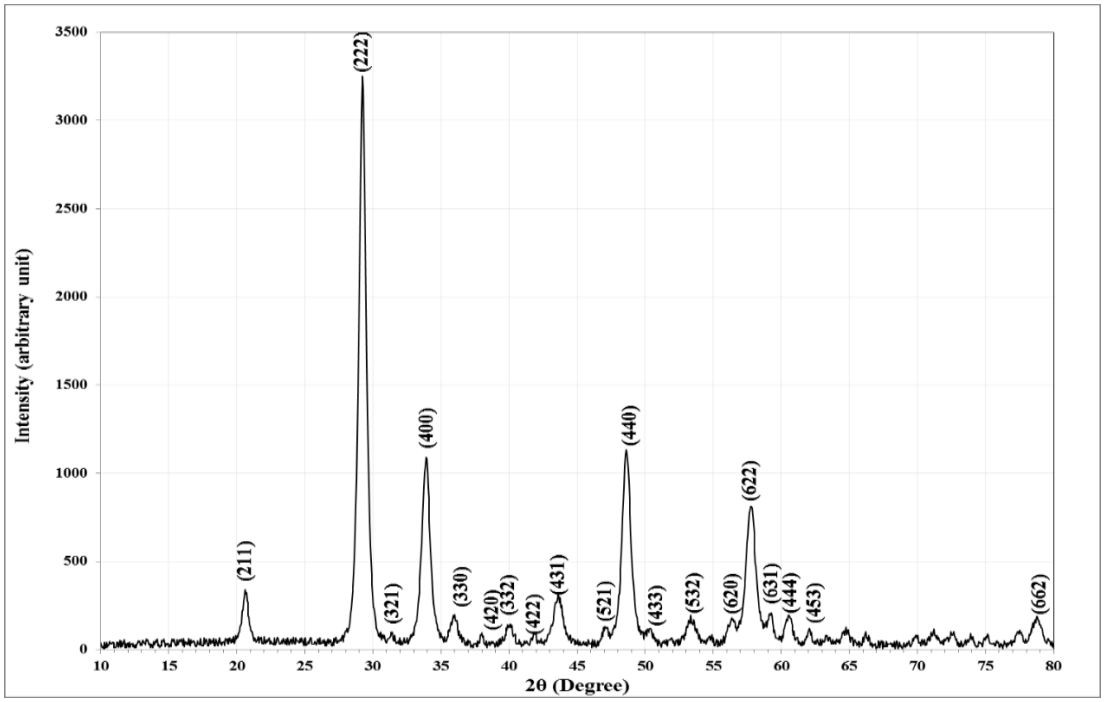

Fig. 11. XRD of Er_2O_3 nanoparticles.

600

601

602

603 Table 1. XRD parameter of Er_2O_3 nanoparticles.

2Ɵ (Deg.)	**FWHM (Deg.)**	**d_{hk1} Exp. (A)**	**G.S. (nm)**	**Hk1**	**d_{hk1} $S_{td.}$ (A)**	**Phase**	**Card No.**	***δ***
20.6330	0.4972	4.3013	16.2	(211)	4.3029	Cub.Er_2O_3	96-101-0593	0.0004
29.2389	0.6119	3.0519	13.4	(222)	3.0426	Cub.Er_2O_3	96-101-0593	0.0031
31.4191	0.3060	2.8449	27.0	(321)	2.8169	Cub.Er_2O_3	96-101-0593	0.0100
33.9052	0.6884	2.6418	12.1	(400)	2.6350	Cub.Er_2O_3	96-101-0593	0.0026
35.9706	0.6120	2.4947	13.7	(330)	2.4843	Cub.Er_2O_3	96-101-0593	0.0042
37.9978	0.2677	2.3661	31.4	(420)	2.3568	Cub.Er_2O_3	96-101-0593	0.0040
40.0249	0.6119	2.2509	13.8	(332)	2.2471	Cub.Er_2O_3	96-101-0593	0.0017
43.6203	0.8032	2.0733	10.7	(431)	2.0671	Cub.Er_2O_3	96-101-0593	0.0030
47.0626	0.4208	1.9294	20.6	(521)	1.9243	Cub.Er_2O_3	96-101-0593	0.0026
48.6308	0.7267	1.8708	12.0	(440)	1.8632	Cub.Er_2O_3	96-101-0593	0.0041
50.3137	0.5737	1.8121	15.3	(433)	1.8076	Cub.Er_2O_3	96-101-0593	0.0025
53.3736	0.7650	1.7152	11.6	(532)	1.7098	Cub.Er_2O_3	96-101-0593	0.0031
56.3187	0.6120	1.6322	14.7	(620)	1.6665	Cub.Er_2O_3	96-101-0593	0.0206
57.7722	0.8032	1.5946	11.3	(622)	1.5890	Cub.Er_2O_3	96-101-0593	0.0035
59.1874	0.4972	1.5598	18.4	(631)	1.5540	Cub.Er_2O_3	96-101-0593	0.0037
60.5643	0.6120	1.5276	15.0	(444)	1.5213	Cub.Er_2O_3	96-101-0593	0.0041
62.0560	0.4590	1.4944	20.2	(543)	1.4906	Cub.Er_2O_3	96-101-0593	0.0026
78.7705	0.8032	1.2140	12.8	(662)	1.2090	Cub.Er_2O_3	96-101-0593	0.0041

604